

Buffering of mantle conditions through water cycling and thermal feedbacks maintains magmatism over geologic time

Johnny Seales¹ [✉], Adrian Lenardic¹ & Mark Richards²

The Earth has remained magmatically and volcanically active over its full geologic history despite continued planetary cooling and a lack of thermal equilibrium in the mantle. Here we investigate this conundrum using data-constrained numerical models of deep-water cycling and thermal history. We find that the homologous temperature - the ratio of upper mantle to melting temperatures - initially declined but has been buffered at a nearly constant value since 2.5-2.0 billion years ago. Melt buffering is a result of the dependence of melting temperature and mantle viscosity on both mantle temperature and water content. We show that thermal and water cycling feedbacks lead to a self-regulated mantle evolution, characterised by a near-constant mantle viscosity. This occurs even though the mantle remains far from thermal equilibrium. The added feedback from water-dependent melting allows magmatism to be co-buffered over geological time. Thus, we propose that coupled thermal and water cycling feedbacks have maintained melting on Earth and associated volcanic/magmatic activity.

¹Rice University, Houston, TX, USA. ²University of Washington, Seattle, WA, USA. ✉email: johnny.seales@gmail.com

It has long been noted that the temperature of Earth's shallow mantle is remarkably close to the melting temperature of rock¹. This is reflected in Fig. 1a, which plots the Earth's average temperature versus depth profile (the geotherm) and rock melting temperatures (the solidus). The proximity of the geotherm and the solidus could be a coincidence. Alternatively, the closeness of the two profiles likely reflects some form of feedback(s) that allow the Earth's cooling and magmatic potential to be co-buffered. Magmatic/volcanic regulation over geologic time has not generally been considered. However, data constraints on melt fraction from continental arcs indicate that magmatic/volcanic regulation is a viable hypothesis (Fig. 1b). The melting data from Keller and Schoene² are consistent with the idea that Earth experienced a decline in magmatic potential since early in its history, leveling off to quasi-steady state around 2.0 to 2.5 billion years ago. A quasi-steady state evolution in the face of continued planetary cooling requires some form of regulating feedback(s). This connects magmatic history to another long-standing issue: Are Earth's thermal and dynamic evolutions self-regulated?

A class of planetary cooling models does allow for thermal self-regulation^{3–5}. A feedback between temperature and planetary cooling rate, facilitated by the temperature-dependence of mantle viscosity, allows the internal temperature of Earth to track the decay of radiogenic heat sources. This maintains the ratio of heat generation to heat loss, termed the Urey ratio (Ur), near unity. However, this regulation mechanism is not directly connected to magmatic evolution¹. More problematic, such models cannot account for updated constraints on Earth's cooling history^{6,7}. In particular, data constraints place Ur between 0.2 and 0.5⁸, i.e., heat loss and heat generation are far from equilibrium.

Self-regulation relates to the reactance time of the solid planet^{9,10}. Reactance time characterizes responses to deviations from a secular cooling trend. The secular trend is associated with the time scale over which the driving energy source for mantle convection changes due to radiogenic decay. Cooling histories that allow for thermal self-regulation have short reactance times relative to the decay time. Short thermal reactance times cannot lead to low Ur values, as they damp large deviations from thermal equilibrium. This, in turn, has been used to argue that mantle convection is not self-regulated, which has implications not only for understanding our own planet's evolution, but also for comparative planetology⁹. Although this argument is robust for

thermal self-regulation, it does not rule out self-regulation altogether.

The ability of a planet to self-regulate depends on a relationship between the vigor of mantle convection, as characterized by the mantle Rayleigh number (Ra), and convective heat flux (Nu). That relationship is given by

$$Nu \sim Ra^\beta \quad (1)$$

where

$$Ra = \frac{\rho g \alpha \Delta T Z^3}{\kappa \eta} \quad (2)$$

where ρ is the density, α is the thermal expansivity, g is the acceleration due to gravity, ΔT is the driving temperature, Z is the thickness of the convecting layer, κ is the thermal diffusivity, and η is the mantle viscosity. Models that allow for thermal self-regulation invoke a strong relationship between Nu and Ra ³, that is, β values near the high-end limit of $1/3$ ⁵. Physically, this means that mantle viscosity is the dominant resistance to tectonic plate overturn. Conceptually, the regulating feedback works as follows: If fluctuations cause heat flux to become low relative to internal heat generation then the mantle will heat up, viscosity will decrease, and heat flux will increase (due to increased convective vigor as a result of lower viscous resistance). The feedback operates on a short time scale relative to secular radiogenic heat source decay. As a result, interior cooling evolves along a series of quasi-equilibrium steps⁴. This is equivalent to Ur remaining near unity. Models with $\beta \leq 0$ can match Ur constraints as they have long thermal reactance times that allow the Earth to remain far from thermal equilibrium^{6,7,9}. Low or negative β indicates that the dominant resistance to mantle convection and plate motion does not come from mantle viscosity, but instead from the strength of plates and/or plate margins. This connects self-regulation to the balance of plate tectonic forces. That balance is not agreed upon and it is critical to developing a dynamic theory of plate tectonics¹¹.

Although classic thermal history studies focused on thermal regulation, the critical assumption at their core is viscosity-regulation. That is, changes in viscosity dominate changes in the Earth's Rayleigh number and, over time scales shorter than secular decay times, viscosity, so that by association the Rayleigh number, can be approximated as remaining constant. This is a critical assumption in using $Nu \sim Ra^\beta$ scaling relationships to

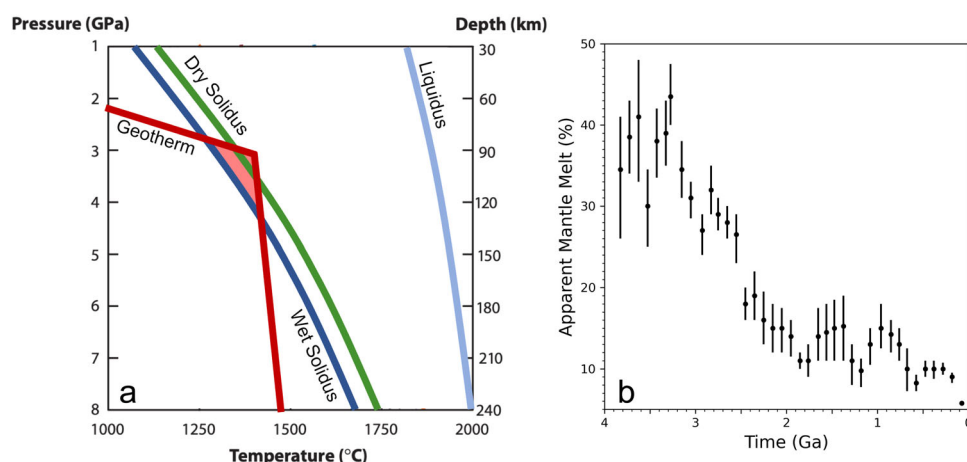


Fig. 1 The extent of mantle melting is controlled by the relative position of a few thermal profiles and is constrained over Earth's history. **a** The position of the Earth's mean oceanic geotherm (red) relative to the dry (green) and wet solidus (dark blue) and liquidus (light blue) of the upper mantle. The geotherm is calculated for a present-day heat flow of 35 TW and a mantle potential temperature of 1350 °C (see "Methods"). The melting curves represent the dry solidus³⁹ and wet solidus¹⁵ assuming 2.5 ocean masses in the mantle. **b** Apparent mantle melt fraction (dots as means and bars as uncertainty) from continental arcs over geologic history^{2,28}.

begin with, as they are based on theory, experiments, and/or numerical simulations carried out under constant Ra values¹². If viscosity depends only on temperature, then a lack of thermal-regulation rules out self-regulation. If that is not the case then self-regulation remains viable. The dependence of mantle viscosity on water opens this possibility^{13,14}. It also allows for potential co-regulation of mantle melting, as increasing mantle water content suppresses the melting temperature of rock¹⁵.

The first generation of thermal history models that considered the role of water predicted Ur values greater than one¹⁶ or comparable to classic models¹⁷. The former enforced a net loss of water from the Earth's interior. The latter assumed that Ur should be 0.8 and, as such, calibrated free parameters to keep mantle water content nearly constant. Crowley et al.¹⁸ elegantly showed that a larger range of behavior is possible if the system allows for imbalances in mantle dewatering (D) and rewatering (R). Mantle dewatering occurs at mid-ocean ridges. The rate of mantle water loss depends on the relative positioning of the solidus and geotherm. Mantle rewatering occurs at subduction zones, where descending slabs carry some of their bound water into the mantle. How much water the slab can carry scales with its thickness, which will increase as the mantle cools. If mantle viscosity depends on temperature (T) and mantle water content (χ), then the time rate of change of mantle viscosity can be written as

$$\frac{d\eta}{dt} = \frac{\partial\eta}{\partial T} \frac{dT}{dt} + \frac{\partial\eta}{\partial\chi} \frac{d\chi}{dt}. \quad (3)$$

Conservation of energy leads to

$$\frac{dT}{dt} = \frac{1}{\rho C_p V} (H - Q_s) \quad (4)$$

where C_p is the specific heat, V is the mantle volume, H is the mantle heat production, and Q_s is the surface heat flow. Conservation of mantle water content leads to

$$\frac{d\chi}{dt} = \frac{1}{\rho V} (R - D). \quad (5)$$

Following the assumption that viscosity remains statistically steady, relative to the time scale over which large changes occur in internal heat generation, leads to an estimate for the Urey ratio given by

$$Ur \approx 1 - \frac{\eta_\chi C_p}{\eta_T Q_s} (R - D), \quad (6)$$

where $\eta_\chi = \frac{\partial\eta}{\partial\chi}$ and $\eta_T = \frac{\partial\eta}{\partial T}$. If R exceeds D , then the Earth can be out of thermal equilibrium and low values of Ur are viable without requiring a weak, or negative, relationship between surface heat loss and Ra . The analysis of Crowley et al.¹⁸ showed that a lack of thermal self-regulation did not rule out the possibility of a more general form of viscosity self-regulation. A subsequent study used coupled thermal history and water cycling models to show that such a mode of self-regulation could lead to cooling paths for the Earth that are consistent with petrological data constraints¹⁹. Those models did not address magmatic evolution, a goal of what follows. A further limitation was that parameter uncertainties restricted the ability to evaluate the robustness of conclusions (i.e., self-regulation could be shown to be plausible, but it could not be shown to be statistically likely given inherent model uncertainties). As such, we have reformulated the forward models into a data constrained inverse approach that allows for the generation of a large number of successful model paths to test the statistical robustness of viscosity self-regulation and its ability to co-regulate magmatic potential.

In the following analysis we employ a new modeling methodology to understand how changes in the deep-water cycle affect

melting of the upper mantle and regulation of mantle convection. We describe the full model in the appendix and cover its critical elements here. Thermal history models employ an energy balance that tracks how mantle temperature evolves with time. Past thermal history models have assumed a range of parameter values and solved for thermal paths over time. Our approach differs by integrating constraints on mantle potential temperature into our model. We consider a suite of thermal paths that satisfy data constraints and then invert for the associated suites of mantle water histories, under different assumptions as to the principal resisting forces to tectonic plate overturn. The essential insight that allows for this methodology comes back to viscosity regulation. Mantle viscosity evolution influences a range of observables, including melt potential. If one of the factors (temperature) that influences mantle viscosity can be constrained, within uncertainty, then the associated evolution of another factor that influences viscosity (water) can be inverted for, subject to added data constraints (e.g., Urey ratio, surface water volume).

The inverse methodology requires a reformulation of traditional thermal and water cycling approaches as discussed in the appendix. It also requires a wider range of constraints. We enforce a conservation of total water and constrain models to a present day surface water content of one ocean mass. To further constrain solution space, we require that present day mantle viscosities be in the range of 10^{19} – 10^{21} Pa.s. We enforce the present day Ur to fall between 0.2 and 0.5. Doing so determines the model's present day radiogenic concentration under variable assumptions as to the present day value of mantle heat flow (we take 35 TW as a canonical value). The greatest strength of the method is that it reduces the number of free model parameters. In particular, uncertainties about the particular parameterizations of how much water returns to the mantle via subduction and/or how much leaves during melting do not enter directly into the inverse methodology. Stated another way, we invert for mantle water history paths that can match observational constraints, which eliminates assumptions regarding mantle dewatering and/or rewatering efficiencies. The parameter space reduction allowed us to find a far larger number of model paths that could satisfy data constraints as compared to the traditional forward modeling approach. In our results we show the output of 10,000 model evolutions that matched data constraints within the uncertainty of the data. A similar forward modeling approach¹⁹ required hundreds of thousands of model runs to find tens of successful models. Those models hinted at the behavior we uncover here, but the limited number of successful models did not allow for a statistical analysis.

Results

To highlight the role of deep water cycling, for self-regulated mantle convection and melt potential, it will be useful to compare outputs of our coupled thermal and deep-water cycling models to outputs of more traditional thermal history models that do not account for deep-water cycling. Figure 2 shows results from the latter class of models (i.e., models in which only temperature affects mantle viscosity and mantle melting). A range of such models is explored allowing for different assumptions as to the resisting forces for tectonic plate motions²⁰. From the full suite of parameter variations explored, we have only selected those that can match paleo mantle temperature constraints with a χ^2 of approximately unity (Fig. 2a). All of the models lack viscosity buffering (Fig. 2b); mantle viscosity responds to mantle cooling by stiffening, becoming harder to move, producing a decline in convective vigor (Fig. 2c). The purely thermal models also lack a buffering of magmatic potential (Fig. 2d). The solidus remains at a fixed thermal profile. Cooling of the interior moves the

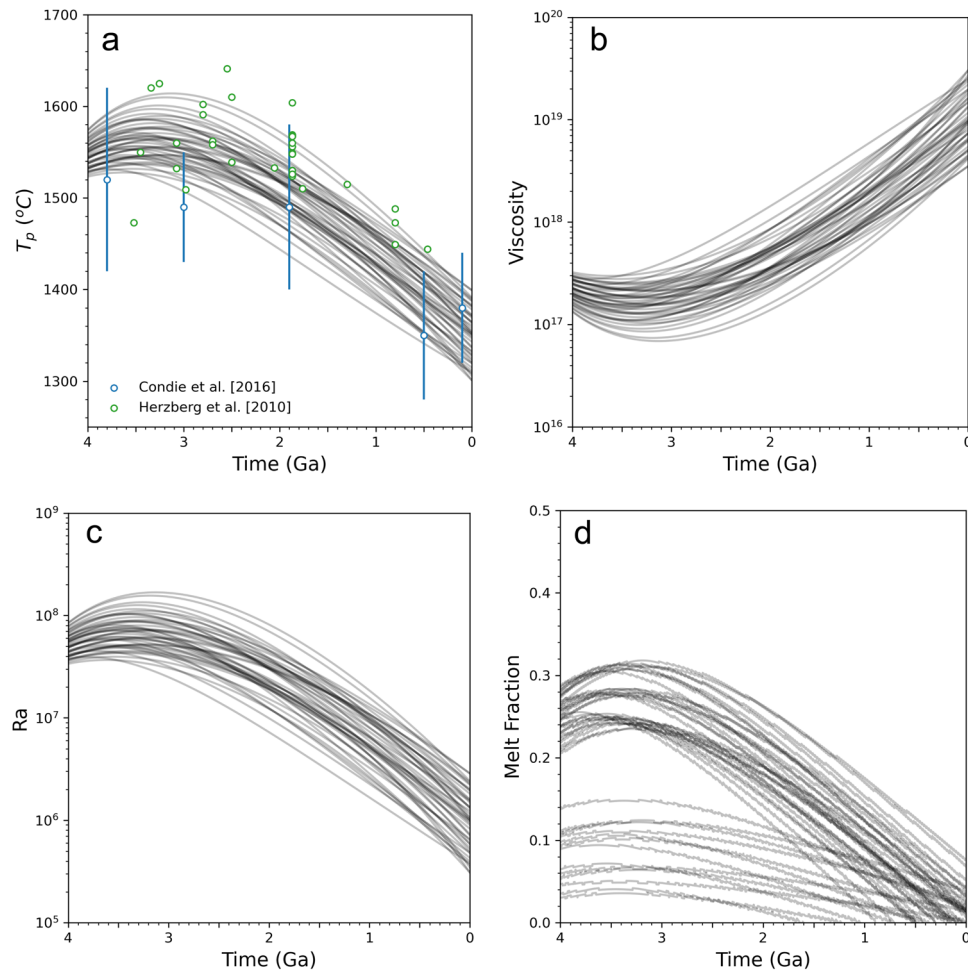


Fig. 2 Thermal history models with deep-water cycling cannot explain melt buffering. **a** Thermal trajectories consistent with data constraints on mantle temperature over geologic time (dots are means and bars uncertainties). **b** Mantle viscosity evolution from the models. Mantle viscosity increases by several orders of magnitude over Earth's history for the models, leading to a decline in convective vigor (Ra) (**c**). **d** Melt fraction paths for the purely thermal models. None of the models allow for melt regulation and many of them predict melt shutdown having already occurred. The two distinct sets of model curves, in the melt path results, are associated with models that assume mantle viscosity dominates resistance to plate overturn (the paths that start with higher melt fractions) versus models that assume that plate and/or plate margin strength provides the dominant resistance (the paths that start with lower melt fractions).

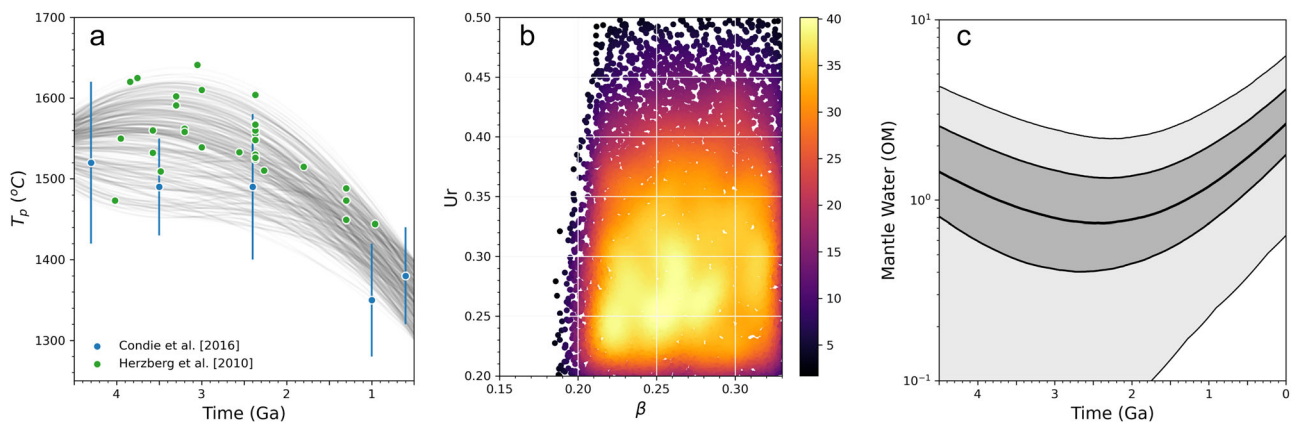


Fig. 3 Constraints on Earth's thermal history require a change from net water loss to water gain at 2–3 Ga. Thermal trajectories consistent with Earth data (**a**) used for obtaining inversion results. **b** Successful Ur – β parameter space colored by relative point density with higher values meaning the density of points is larger. **c** Distribution of mantle water content about its median value, with the dark gray indicating values falling between the upper and lower quartiles and the lighter gray constraining the maximal and minimal limits.

geotherm to cooler temperatures, towards the solidus, producing a continual decline in mantle melting.

Figure 3 shows model thermal constraints and model outputs for coupled thermal and deep water cycling models. The set of thermal trajectories (>250) depicted in Fig. 3a satisfied a goodness of fit test between each trajectory and petrological data constraints (see appendix). The thermal trajectories served as constraints for our inversion scheme. We generated 10,000 successful mantle water history inversions consistent with data constraints by randomly sampling different combinations of β and Ur for the full family of thermal trajectories. Data constraints require present day Ur values between 0.2 and 0.5. Our sampling required β take a positive value less than or equal to 0.33 but remain in the positive domain. Figure 3b shows the relative density of β - and Ur -space from successful models. Only β values exceeding approximately 0.2 produced model results that matched all data constraints. It has been argued that thermal history models with β values in this range produce a thermal catastrophe - the runaway of mantle temperatures to unnaturally high values early in Earth's existence^{6,7}. That argument was applied to models in which only temperature affects mantle viscosity. Adding the effects of deep-water cycling on mantle viscosity removes this perceived weakness of high β value models, as they can match Urey ratio constraints without requiring excessively high mantle temperatures in the past.

Figure 3c shows mantle water histories that satisfy data constraints, within uncertainty bounds. Unlike previous thermal history models, which tend to show handfuls of single trajectory paths, our methodology allows us to plot the probability distribution for 1000s of successful model paths. This, in turn, quantifies how coupled data and model uncertainty affect results and provides a measure for the robustness of model based conclusions. The thick, black lines represents the median mantle water history. The darker region extends from the upper to the lower quartile. The lighter regions extend outwards from these quartiles a distance of one and half times the interquartile range. Figure 3c indicates a preferential loss of water from the mantle over its early evolution and a shift to preferential ingestion of water into the mantle between two and three billion years ago. More water brought in through subduction than was lost through melting at mid-ocean ridges. That shift from net mantle dewatering to rewatering temporally coincides with the findings of Parai and Mukhopadhyay²¹ and Seales and Lenardic¹⁹ and with inferences that a shift from hot and dry to cold and wet subduction occurred in that time window^{22,23}. Dong et al.²⁴ suggested a net rewatering over a larger portion of Earth's history by estimating mantle water capacitance. This, however, is based on an estimate for an upper limit for mantle water storage and the assumption that the mantle is always at its water storage limit. We know of no physical reasoning demanding that the mantle remain at this limit. Furthermore, the majority of our results fall within or below the uncertainties of Dong et al.²⁴ (i.e., the studies are consistent within data uncertainties).

Figure 4a shows the evolution of mantle viscosity from successful models. Successful models show an increase in mantle viscosity for roughly the first half of Earth's history followed by a milder decline. The rollover coincides with the change from net mantle dewatering to rewatering. Preceding the rollover, mantle melting stiffened the mantle, whereas once subduction began to outpace water loss at the ridges, the mantle became wetter. The changes in mantle viscosity are mild. This indicates self-regulation via coupled thermal and water cycling feedbacks. The mild changes in mantle viscosity lead to associated mild changes in mantle convective vigor, a measure of which is Ra . Figure 4b shows the uncertainty in the evolution of Ra . Mantle vigor mildly declined during the net dewatering phase and mildly

increased during the net rewatering phase. The results show that mantle evolutions with mild changes in convective vigor are consistent with data constraints and, within coupled data and model uncertainties, are statistically more likely than paths with large changes in convective vigor. Mild changes in Ra , in the face of a large decline of internal radiogenic heating, indicate a self-regulating mantle.

Although mantle self-regulation has been suggested in the past, to the best of our knowledge the hypothesis of a nearly constant level of convective vigor over geologic time is new. Previous ideas regarding self-regulation invoked a negative thermal feedback that would damp short time scale perturbations in mantle evolution. A warm thermal perturbation would decrease viscosity, leading to increased convective vigor, amplifying heat loss and bringing mantle temperature back into a quasi-steady state. Such a feedback leads to mantle heat flow and Ra tracking the decay of radiogenic heat sources over time³⁻⁵. The value of Ra would monotonically decline as the planet aged. The idea that convective vigor itself could be regulated at a near constant value, despite decreases in the driving force of convection, has not been proposed to date.

Our analysis shows that the combined effects of temperature and water on mantle viscosity allow for a deeper level of self-regulation, reflected by a relatively flat, and potentially increasing, Ra trend (Fig. 4b). As well as being consistent with a range of thermal data constraints, as laid out above, this form of self-regulation is also consistent with inferences of tectonic plate velocities over geologic time. In an analysis of passive margins, Bradley²⁵ found that the history of passive margins indicated that plate speeds have not been decreasing over geologic time. Within data uncertainty, plate speeds may have even be increasing. Condie et al.²⁶ also argued that tectonic plate speeds have not changed considerably over geologic time based on an analysis of paleo-magnetic data and the history of super-continent amalgamation and dispersal. Near constant, and potentially increasing, plate speeds over geologic time is difficult to explain if the vigor of mantle convection has decreased over time. It is, however, a predicted result from a self-regulated mantle evolution that buffers mantle viscosity over geologic time. That mode of self-regulation is also consistent with the conjecture, based on observational constraints on water transport beneath Japan arcs, that deep-water cycling could stabilize and prolong mantle convection and the associated geological activity of the Earth²⁷.

Self-regulation of mantle viscosity, and convective vigor, does not necessarily lead to an equivalent buffering of mantle melt potential over geologic time. The evolution of a homologous temperature, a ratio of temperature to melting temperature, can be used to assess whether viscosity self-regulation can lead to an associated regulation of mantle melt potential. The mantle homologous temperature (T_H) is defined as the ratio of the mantle geotherm and the wet solidus. Figure 1a shows these profiles in red and dark blue, respectively. The two profiles change with depth. The maximum distance between the two curves occurs at the base of the thermal lithosphere (see Methods). The greater the thermal distance between the solidus and geotherm, the greater the value of T_H , and the more melting that occurs in the upper mantle.

Figure 5 shows how T_H evolves for successful models. Preferential loss of water from the mantle (Fig. 3c) shifted the solidus to warmer temperatures during the first few billion years of Earth's history. Mantle temperature changed little during this period. The thermal distance between the solidus and geotherm decreased, leading to a proportional drop in T_H . The decline eased when subduction began bringing in more water than was lost from melting at the ridges around 2 Ga when mantle temperatures were falling mildly. Flattening of T_H indicates a near

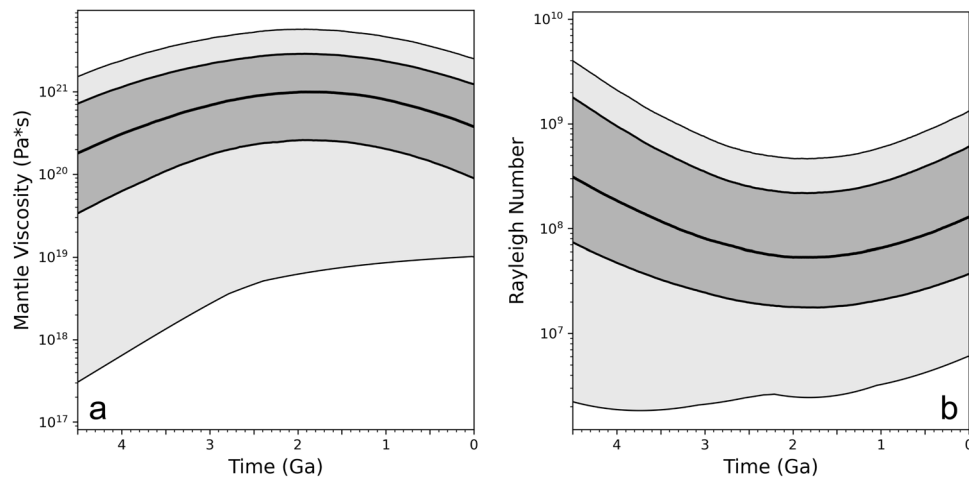


Fig. 4 Measures of mantle self-regulation. **a** Inversion results showing mild changes in mantle viscosity and its impact on convective vigor (Ra) (**b**) throughout Earth's history. Each figure plots results as distributions about a median value. The darker color highlights values falling between the upper and lower quartiles and the lighter color constraining the maximal and minimal limits.

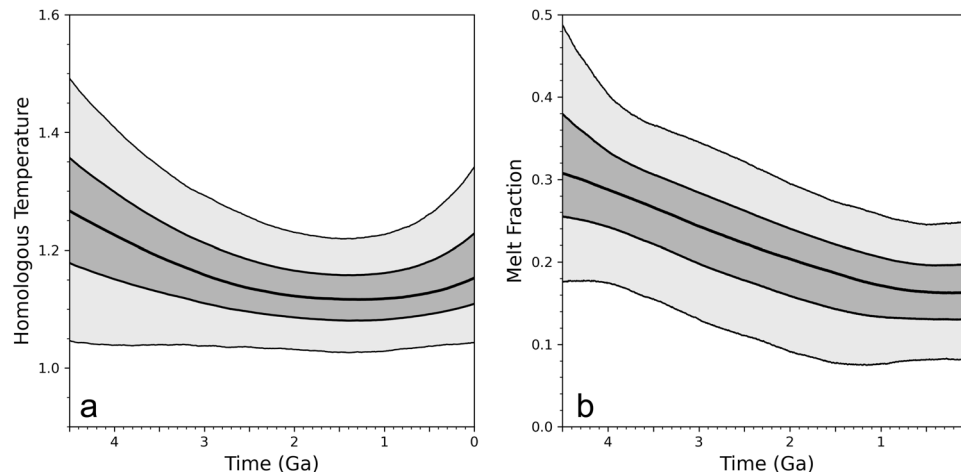


Fig. 5 Measures of melt co-regulation due to changes in viscous self-regulation. **a** Inversion results for the homologous temperature (T_H), the ratio of the geotherm and wet solidus at the base of the lithosphere (**b**) Inversion results for melt fraction showing a decline for billions of years followed by a leveling off near present day. Each of the figures show results as distributions about their median value. The darker color highlights values falling between the upper and lower quartiles and the lighter color constraining the maximal and minimal limits.

constant thermal distance between the solidus and geotherm. Flattening persisted until the most recent few hundred million years, during which it slowly increased - this occurred as the solidus began to move toward cooler temperatures faster than the geotherm.

The co-evolution of the solidus and geotherm feeds into the evolution of mantle melting as plotted in Fig. 5b. Melt fraction, a measure of mantle melting, mirrors the qualitative behavior of homologous temperature: it peaks early in Earth's history and regulates towards present day. Peak melting coincided with warm mantle temperatures and high mantle water content. Declining water content and relatively fixed temperatures produced a decline in melting by bringing the solidus closer to the geotherm. The change from preferential mantle water loss to gain did not immediately impact melt fraction the way it did homologous temperature. Melt fraction declined until around one billion years ago, after which it flattened. Homologous temperature became regulated when the thermal distance between the solidus and geotherm settled into a relatively constant value. The solidus and geotherm maintained this thermal distance and initially moved towards cooler temperatures at roughly the same rate. Melting

continued to decline even though T_H remained constant. The required increase in mantle water content to regulate mantle viscosity caused the solidus to move towards cooler temperatures faster than the geotherm, causing melt fraction to become buffered at a near constant value. Melt buffering, then, is directly tied to the self-regulation of mantle viscosity.

Discussion

Unlike purely thermal models (Fig. 2d), models that allow for deep water cycling (Fig. 5b) predict that mantle melt potential has been buffered over the last 2 billion years, consistent with data of Keller and Schoene²⁸. Returning to a motivating observation for our study, this is consistent with the hypothesis that the present-day proximity of the mantle geotherm to the solidus is not a coincidence, but reflects the coupled thermal history and deep-water cycling feedbacks that buffer mantle viscosity and mantle melting.

The hypotheses that deep water cycling buffers mantle thermal and magmatic evolution is bolstered by the fact that the deep water cycling models are also compatible with a range of added data constraints. This includes constraints on the internal mantle

temperature, surface water volume, mantle water volume, mantle viscosity, mantle Urey ratio and inferences on the change of tectonic plate speeds over geologic time. The inferred balance of resisting forces to plate motions, from successful water cycling models (Fig. 3b), is also consistent with more detailed models of subduction zone dynamics²⁹.

Self-regulation does not require that mantle viscosity and/or melt production remain constant. Fluctuations can occur, but negative feedbacks tend to bring the system back toward a mean trend. For example, the Earth's thermal-tectonic system allows for fluctuations due to the chaotic nature of mantle convection, changes in plate dimensions, and the amalgamation/dispersal of super-continentals. These fluctuations can lead to variations in deep water cycling³⁰. Fluctuations could also occur as a result of variations in the time scale of mixing water into the mantle³¹. The buffering feedbacks in the coupled thermal and deep-water cycling system can still maintain a self-regulated evolution in a statistical sense. That is, fluctuations cause variations about a mean trend but buffering feedbacks do not allow for runways and or long-lived departures from a buffered trend (see Methods). This is consistent with the data of Keller and Schoene²⁸, which show fluctuations in melt fraction about a slowly varying mean trend over the last 2 billion years (Fig. 1b). In principle, one could incorporate added data constraints into our models based on, for example, fluctuations in mantle potential temperature³² and/or mean plate subduction age³⁰, but that goes beyond our scope here.

As well as buffering viscosity and magmatism over the last 2 billion years, water cycling can continue to do so into Earth's future. That said, the trends of Fig. 5b cannot extend indefinitely. Exactly when self-regulated, melt buffering will end depends on the future path of mantle temperature and water content. Given that the solidus depends on water content, the self-regulation mechanisms mapped herein can delay melt shutdown relative to a dry planet or to a planet that does not allow for deep water cycling effects on mantle evolution (Fig. 2d). In principle, we could extend our models forward in time. The results would, however, be deceptive as we would be taking a data assimilation method outside of data constraints. This leads to increasing uncertainty the further a projection is taken outside of the data³³. The inverse models could be augmented with forward models, subject to uncertainty quantification^{10,20}, to provide probability densities for the timing of melt shut down. That type of analysis would also need to consider the potential of cooling-induced shifts in tectonic modes from plate tectonics to a single plate planet. That goes beyond the intent of this paper (i.e., to investigate the hypothesis that mantle melting was self-regulated over the Earth's evolution to the present day).

Our models, like any others, make simplifying assumptions about some processes and exclude others entirely. One simplification, shared by the majority of thermal history models, is that only mean trends are tracked. Temperature and water content have likely fluctuated about mean trends over Earth's history. Plate age and velocity may not always tightly couple, which would produce a variance in the amount of water delivered into subduction zones, impacting the frequency and magnitude of arc volcanism. The super-continental cycle could produce intermittent thermal gradients within the mantle, allowing plate velocities and mixing time scales to deviate from mean trends. Although we have shown that self-regulation can exist under fluctuations, it would be of value to account for the specific sources of fluctuations noted above to see how they affect evolution trends. An added source of fluctuations, that could be explored, is associated with changes in the dominant resistance to plate motions. In our model formulation this is parameterized as the β scaling factor in the relationships between convective vigor

and mantle cooling and between convective vigor and plate speeds. Although we explored a range of β values, all our models assumed a constant value over a single model path. That assumption could be relaxed to provide a deeper exploration of how tectonic fluctuations affect our model trends. An added effect that could be incorporated into our models is continental growth. Continental growth will partition radiogenics between the mantle and continents, which will affect thermal history. Models that include continental growth will still need to match all the data constraints we have laid out but it is likely that not all potential continental growth curves will be able to do so. This could provide a means to use our modeling methodology to discriminate between competing continental growth hypotheses.

All of our models have assumed that plate tectonics has operated over all of geologic time and that plate subduction is the dominant means of mantle cooling. As we noted, extending our models forward in time, to explore the potential longevity of magmatic self-regulation, will require allowing for the potential of tectonic transitions. This could also be of value for extending the scope of the models for the Archean Earth. Under Archean thermal conditions it is possible that latent heat effects and the advection of magma from the interior mantle to the surface could become important effects for mantle cooling³⁴. Another future avenue is comparing how our results scale to higher dimension models. Higher dimension models would also allow for a more direct means of tracking potential tectonic transitions. That would be of utility not only for extending the range of early Earth processes our models could incorporate but also for comparative planetology studies that explore how different tectonic modes, and potential transitions between them, affect water cycling and thermal evolution of terrestrial planets that have evolved differently than the Earth.

We can hypothesize at this stage that self-regulation as we have defined it requires bidirectional cycling of water. Take as an endmember a stagnant lid planet that does not recycle water into the mantle. The planet would continuously lose water from its interior throughout its magmatic lifetime. Such behavior would prohibit the solidus and geotherm to both evolve towards lower temperatures; As decaying radiogenics produced less heat in the mantle, the interior would likely cool, causing a convergence between the solidus and geotherm. Considering only this one effect suggests that planets with a bidirectional deep-water cycle, such as Earth, have the potential for experiencing self-regulation compared to a planet having a unidirectional deep-water cycle. This hypothesis can be tested by expanding the methodology used in this study along with constraints on the evolution of a stagnant lid planet, such as Mars.

Conclusions

Data-constrained models of Earth's thermal history indicate that coupled deep-water and thermal cycles can lead to a self-regulated mode of mantle convection with an associated self-regulation of the Earth's magmatic potential. Fundamentally, partial melting in Earth's upper mantle (asthenosphere), due to the presence of volatiles, mode locks the mantle toward higher (nearer wet solidus) interior temperatures, and hence higher heat flow and a lower Urey ratio, relative to a planet that lacks deep water cycling. This conclusion is likely to have important implications for Earth's plate tectonic style of mantle convection, in that partial melting in the asthenosphere profoundly influences the existence and behavior of plates and plate motions—indeed sound arguments can be made that the long-term persistence of plate tectonics on Earth requires the persistence of a partially molten uppermost mantle. We further suggest that exploration of both constraints for and models of mantle dewatering and

rewatering (related primarily to volatile processing at ridges and subduction zones) should shed further light on mantle evolution and self-regulation.

Methods

Assimilating data into parameterized thermal history models. The average mantle temperature changes with time (\dot{T}_m) according to the balance of heat produced within (H) and lost from (Q) the mantle:

$$\rho V c_p \dot{T}_m = H - Q \tag{7}$$

where V and c_p are the volume and heat capacity of the mantle, respectively³⁵. This energy balance neglects any heat transferred from the core into the mantle. The amount of heat produced by the decay of radiogenic elements within the mantle scales as

$$H = V h_i \exp(-\lambda t) \tag{8}$$

where h_i is the initial heat generation rate, λ is the decay constant, and t is time. We ignore the partitioning of radioactive elements between the mantle and crust. The total amount of heat lost by convective cooling is

$$Q = A q_m \tag{9}$$

where A is the surface area of the convecting mantle and q_m the convective heat flux. Non-dimensional heat flux (Nu) scales with the Rayleigh number (Ra), a measure of convective vigor, according to

$$Nu = \frac{q_m}{q_{cond}} = \left(\frac{Ra}{Ra_c} \right)^\beta \tag{10}$$

where q_{cond} is the amount of heat lost were it transferred solely by conduction through the entire layer, Ra_c is the critical Rayleigh number and β is a scaling exponent. The parameter β varies between models that make different assumptions as to the dominant forces resisting tectonic plate motion (see Seales and Lenardic²⁰ for a fuller discussion of what different β values mean for mantle convection). Fourier's law states that

$$q_{cond} = k \frac{\Delta T}{Z} \tag{11}$$

where k is the thermal conductivity of the mantle, Z is the depth of the convecting layer, and ΔT is the temperature difference driving convection. The latter is the difference between the surface temperature (T_s) and the average mantle temperature. Combining Eqs. (10) and (11) and rearranging, the convective heat flux is

$$q_m = k \frac{\Delta T}{Z} \left(\frac{Ra}{Ra_c} \right)^\beta \tag{12}$$

where Ra is

$$Ra = \frac{\rho g \alpha \Delta T Z^3}{\kappa \eta} \tag{13}$$

and α is the mantle thermal expansivity, κ is the mantle thermal diffusivity, and η is the mantle viscosity. Note that when classic boundary layer theory is assumed ($\beta = 1/3$), Z vanishes. Reducing the value of β negates this effect and results in an inverse relationship between q_m and Z . Changes in mantle viscosity dominate changes in Ra . The viscosity is given by

$$\eta = \eta_o A_{cre}^{-1} [\exp(c_0 + c_1 \ln \chi_m + c_2 \ln^2 \chi_m + c_3 \ln^3 \chi_m)]^{-r} \exp\left(\frac{E}{RT_m}\right) \tag{14}$$

where η_o is a scaling constant, c_1 , c_2 and c_3 are empirically determined constants¹⁴, r is the water fugacity exponent, A_{cre} is a material constant, E is the activation energy for creep and R is the universal gas constant. In Eq. (14), χ_m has units $H/10^6$ SI.

Combining Eqs. (7) to (13), we find that the change in mantle temperature evolves according to

$$\dot{T}_m = \frac{1}{\rho c_p} \left[\sum_{i=1}^n h_i \exp(-\lambda_i t) - \frac{A}{V} \frac{k \Delta T}{D} \left(\frac{\rho g \alpha \Delta T D^3}{Ra_c \kappa \eta} \right)^\beta \right] \tag{15}$$

Rearranging to isolate mantle viscosity, Eq. (15) becomes

$$\eta = \frac{Ra_c \kappa}{\rho g \alpha \Delta T D^3} \left[\frac{V}{A} \frac{D}{k \Delta T} \left(\sum_{i=1}^n h_i \exp(-\lambda_i t) - \rho c_p \dot{T}_m \right) \right]^{-\frac{1}{\beta}} \tag{16}$$

Equations (14) and (16) have η isolated. As such, we can use these equations to estimate χ_m . We use Herzberg et al.³⁶ and Condie et al.³⁷ as constraints on T_m . Viable thermal paths based on those T_m constraints (Section "Constructing thermal trajectories") provide constraints on the time derivative of mantle temperature (\dot{T}_m). The Urey ratio, defined as $Ur = H/Q$, serves as a data constraint. Given a present day estimate of Q , we can calculate present day H . Substituting this value of H into Eq. (8), we can rearrange and solve for h_i , which will determine the rate of radiogenic heating for that model. Given the parameters in Table 1 and the constraints laid out here, χ_m remains the only unknown in Eqs. (14) and (16). We

Table 1 Model parameters and values.

Parameter	Description	Value	Unit
ρ	Mantle density	3000	kg m ⁻³
c_p	Mantle heat capacity	1400	J (kg K) ⁻¹
k	Mantle thermal conductivity	4.2	W (m K) ⁻¹
α	Mantle thermal expansivity	3×10^{-5}	K ⁻¹
κ	Mantle thermal diffusivity	10^{-6}	m ² s ⁻¹
λ	Radiogenic decay constant	3.4×10^{-10}	yr ⁻¹
Q_i	Present day mantle heat flow	35×10^{12}	W
Ur	Present day Urey ratio	0.2-0.5	-
β	Convective scaling exponent	0.15-0.33	-
Ra_c	Critical Rayleigh number	1100	-
T_s	Surface Temperature	300	K
g	Acceleration due to gravity	9.8	m s ⁻²
R_p	Radius of Earth's surface	6371000	m
R_c	Radius of Earth's core	3471000	m
Z	Thickness of convecting layer	2900000	m
η_o	Viscosity constant	1.7×10^{17}	Pa s
A_{cre}	Material constant	90	MPa ^{-rs-1}
C_0	Empirically determined viscosity constant	-7.98	-
C_1	Empirically determined viscosity constant	4.35	-
C_2	Empirically determined viscosity constant	-0.57	-
C_3	Empirically determined viscosity constant	0.03	-
E	Creep activation energy	4.8×10^5	J mol ⁻¹
R	Universal gas constant	8.314	J mol ⁻¹
r	Water fugacity exponent	1.2	-
T_o	Starting mantle temperature	1400-1800	°C
T_f	Present-day mantle temperature	1300-1400	°C
T_{m1}	Rollover temperature	1450-1650	°C
τ_{mT}	Rollover temperature	-5 to 25	°C
t_o	Initial model time	0	Gyr
t_f	Final model time	4.5	Gyr
t_{m1}	Intermediate model time	1.25-2.5	Gyr
τ_{mt}	Intermediate model time	0.75-0.25	Gyr
A_f	Temperature fluctuation amplitude	1%	°C
λ_f	Temperature fluctuation decay constant	1/4.5	Gyr ⁻¹
P_f	Temperature fluctuation frequency	1	Gyr ⁻¹
A_1	Anhydrous solidus calibration constant	1085.7	°C
A_2	Anhydrous solidus calibration constant	132.9	°C GPa ⁻¹
A_3	Anhydrous solidus calibration constant	-5.1	°C GPa ⁻²
K	Hydrous solidus calibration constant	43	°C wt%- γ
γ	Hydrous solidus scaling exponent	0.75	-
ϵ	χ convergence tolerance	10^{-8}	Hx10 ⁻⁶ Si
OM	Present day ocean mass equivalent	1.39×10^{21}	kg

initially estimate the mantle water content and then iteratively adjust this value until Eqs. (14) and (16) are within some tolerance (ϵ) of each other. We verified the inversion results against the outputs of forward models. The global maximum inversion error remained less than one percent and the average inversion error remained below 0.01 percent over the modeled time domain.

Constructing thermal trajectories. The method detailed above requires a thermal trajectory as input. One can imagine many trajectories satisfying the uncertainties in estimated mantle potential temperature (Fig. 3a). As such, we constructed a number of data constrained thermal trajectories, each of which passed through

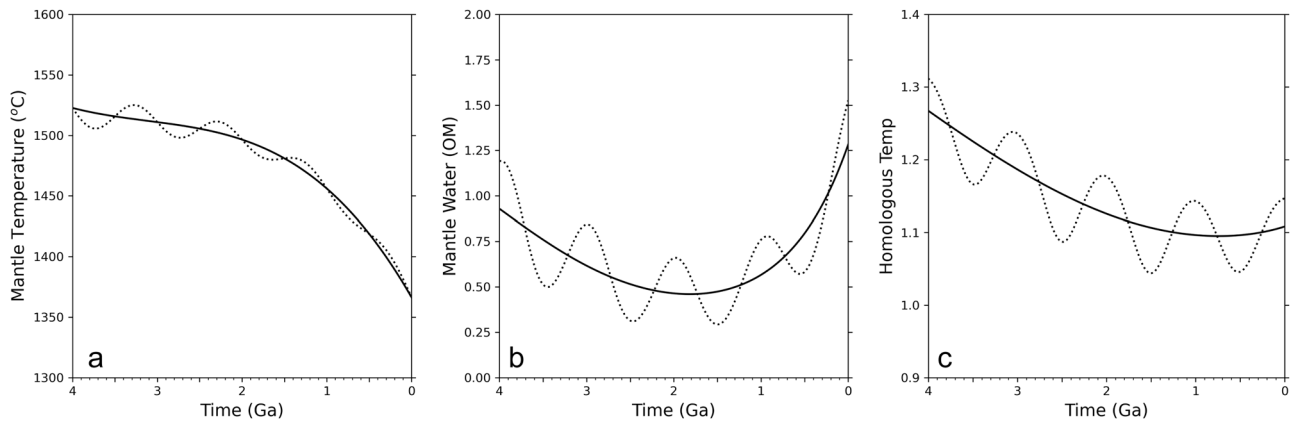


Fig. 6 Analysis of fluctuations on modeling results. Fluctuations in Earth's potential temperature (a) produce an offsetting fluctuation in mantle water content (b). The combined effect is a fluctuating, but quasi-regulated, homologous temperature (c).

strategic control points (p_i) defined by the coordinates (t_i, T_i), with time t_i in billions of years before present and mantle potential temperature T_i in °C. The control points P_o and P_f define the initial and present-day temperatures, respectively. We required each thermal trajectory pass through at least one intermediate control point P_{m1} , which coincides with the rollover in the Herzberg et al.³⁶ and the change in slope of Condie et al.³⁷. Table 1 lists the uncertainties we considered for each control point. We drew random samples from uniform distributions defined by these bounds. These samples served as the starting point of our thermal trajectory. If the sampling resulted in $T_{m1} > T_o$, we defined the thermal trajectory using the quadratic

$$T(t) = \alpha_1 t^2 + \alpha_2 t + \alpha_3. \quad (17)$$

We determined the constants α_i by using the control points P_o , P_{m1} and P_f to form a system of three equations with three unknowns. If sampling resulted in $T_{m1} < T_o$, we defined the thermal trajectory using the cubic

$$T(t) = \alpha_1 t^3 + \alpha_2 t^2 + \alpha_3 t + \alpha_4. \quad (18)$$

Solving for α_i required a system of equations based on four control points. To account for this, we introduced P_{m2} such that $t_{m2} = t_{m1} - \tau_{mt}$ and $T_{m2} = T_{m1} - \tau_{mT}$. Here τ_{mt} and τ_{mT} represent offset times and temperatures. These allow for flattening of the thermal trajectory after an initial temperature decline, which can occur when water and thermal cycles effect mantle viscosity¹⁹.

We required that each thermal trajectory fit the data of Herzberg et al.³⁶ and Condie et al.³⁷ within some measure of goodness. We used a reduced chi-squared statistic, the chi-square (χ^2) per degree of freedom (ν). We adopt χ^2 as traditionally defined:

$$\chi^2 = \sum_t \frac{[D(t) - M(t)]^2}{\sigma(t)}. \quad (19)$$

This cumulatively measures the error ($\sigma(t)$) normalized difference between the data ($D(t)$) and modeled thermal trajectory ($M(t)$). For measuring the goodness of fit we included all data points from both data sets. This gave us a total of 38 data points (N_d). The definition for degrees of freedom is: $\nu = N_d - N_\alpha + N_p$ given the number of parameters (N_α) and control points (N_p). We only kept thermal trajectories that had $\chi^2/\nu < 1$. Using this method, we found a median accepted value of 0.98. As this is nearly unity, so the thermal paths approximate the data error variance without over-fitting.

To mimic a fluctuating mantle temperature, we constructed fluctuations (T_f) that followed the form of an exponentially damped sine wave, which is of the form

$$T_f(t) = A_f e^{-\lambda_f t} \sin\left(\frac{2\pi}{P_f} t\right) \quad (20)$$

where A_f is the amplitude of the sine wave, λ_f is the decay constant, P_f is the period and t is time, in billion of years. We set A_f to one percent of the initial mantle potential temperature, λ_f to 0.22 Gyr^{-1} and P_f to 1 Gyr. We then superimposed T_f on top of a path defined as above. We still enforced the condition that $\chi^2/\nu < 1$. We do not pretend to know what path fluctuations follow. They likely follow something much more complicated than presented here. However, we believe that the qualitative form of our findings will hold. An exact description of the fluctuations is beyond the scope of this paper. How to account for them in forward modeling was covered by Seales et al.¹⁰. Regardless, choosing any other path would find the same qualitative conclusions presented herein.

Homologous temperature. Our analysis relied on the geotherm consisting of two elements: a shallow conductive profile through the mantle lithosphere and a convective profile beneath it. For a given value of T_p and $\chi_{\text{H}_2\text{O}}$, we can calculate q_m

according to Eq. (12). We can rearrange Fourier's Law to give the conductive profile according to

$$T_{\text{cond}}(z) = \frac{q_m}{k_m} z + T_s. \quad (21)$$

The convective profile is the mantle adiabat. We used a linearized version of Mckenzie and Bickle³⁸ above to convert from T_m to T_p . We can also use this adiabat to construct the convective element of the geotherm according to

$$T_{\text{conv}}(z) = T_m \left[1 - \frac{g\alpha}{c_p} \left(\frac{R_p - R_c}{2} - z \right) \right] \quad (22)$$

The conductive and convective profiles intersect at the base of the lithosphere (H_L):

$$H_L = \left[T_m - T_s - \frac{T_m g \alpha}{2 c_p} (R_p - R_c) \right] \left(\frac{q_m}{k_m} - \frac{T_m g \alpha}{c_p} \right)^{-1} \quad (23)$$

In our analysis we compared the geotherm to the solidus. We used the dry solidus of Hirschmann³⁹. We accounted for water suppressing the dry solidus using the parameterization of Katz et al.¹⁵:

$$T_{\text{sol}}(z) = A_1 + A_2 * \rho g z + A_3 (\rho g z)^2 - \Delta T + 273 \quad (24)$$

$$\Delta T(\chi_{\text{H}_2\text{O}}) = K \chi_{\text{H}_2\text{O}}^\gamma \quad (25)$$

where the temperature is given in Kelvin and A_1 , A_2 , A_3 , K and γ are calibration constants.

Generally, a homologous temperature is defined as the ratio of actual temperature to melting temperature. We follow this convention and define the homologous temperature (T_H) as the ratio of the geotherm temperature to the solidus temperature. Both temperatures vary with depth, so we chose the depth that maximized the thermal distance between them—the base of the lithosphere:

$$T_H = \frac{T_{\text{cond}}(H_L)}{T_{\text{sol}}(H_L)} \quad (26)$$

We can insert Z_L into Eq. (21) to get the actual temperature and into Eq. (24) to obtain the melting temperature.

Calculating melt zone thickness. Melt zone thickness (H_M) is defined as the vertical difference between the two points where the geotherm and solidus intersect. The shallower point defines the top of the melt zone (H_T). Equating Eqs. (21) and (21) and gathering like terms gives the quadratic

$$A_T z^2 + B_T z + C_T = 0 \quad (27)$$

$$A_T = A_3 (\rho g)^2 \quad (28)$$

$$B_T = A_2 \rho g - \frac{q_m}{k_m} \quad (29)$$

$$C_T = A_1 - K \chi_{\text{H}_2\text{O}}^\gamma + 273 - T_s \quad (30)$$

This quadratic has two roots, one above the surface (unphysical) and one at depth. The one at depth defines (H_T) and is given by

$$H_T = \frac{-B_T - \sqrt{B_T^2 - 4A_T C_T}}{2A_T} \quad (31)$$

We found the base of the melt zone (H_B) by equating the convective profile (Eq. (21)) with the solidus (Eq. (24)). Grouping like terms and gathering gives the

quadratic

$$A_B z^2 + B_B z + C_B = 0 \quad (32)$$

$$A_B = A_3 (\rho g)^2 \quad (33)$$

$$B_B = A_2 \rho g - \frac{g \alpha}{c_p} T_m \quad (34)$$

$$C_B = A_1 - K_{H_2O}^\gamma + 273 - T_m \left[1 - \frac{g \alpha}{c_p} \left(\frac{R_p - R_c}{2} \right) \right] \quad (35)$$

This quadratic has two roots. The physical root is the shallower of the two. The deeper is an artifact of the chosen solidus structure rather than anything physical. We define the base of the melt zone (H_B), then, as

$$H_B = \frac{-B_B + \sqrt{B_B^2 - 4A_B C_B}}{2A_B} \quad (36)$$

Data constrain the solidus to a depth of 300 km. We set this as a hard maximum limit for H_B .

Calculating melt fraction. The distance between the the solidus and geotherm determines the amount of melt produced. The distance between the solidus and geotherm varies between the top and bottom of the melt zone. As such, we calculate the melt fraction (ϕ) at each depth according to

$$\phi = \frac{T(z) - T_{sol}(z)}{T_{liq}(z) - T_{sol}(z)} \quad (37)$$

assuming that the melt fraction increases linearly between the solidus and liquidus (T_{liq}). We integrate Eq. (37) over the entire melt zone and normalize by melt zone thickness to obtain an estimate of average melt fraction ($\bar{\phi}$).

How fluctuations affect results. Results in the main body of our paper track the evolution of mean trends, together with uncertainties. Self-regulation does not, however, require that planetary variables remain on slowly varying mean paths. Fluctuations can occur but negative feedbacks tend to bring the system back toward a mean trend. Our methodology can deal with the possibility of internal fluctuations. The extended methodology employs a perturbed physics approach, in which fluctuations are imposed on the evolution of a model variable¹⁰. An example can demonstrate the effects of including fluctuations in our analysis by comparing smooth to fluctuating thermal paths (Fig. 6a). The particular form of fluctuations is an example only. Figure 6b, c shows how thermal fluctuations affect water cycling and melt potential, respectively. The system maintains a self-regulated evolution but it does so in a statistical sense (note that this would not be the case if positive feedbacks dominated the system and or if negative feedbacks were overly weak). As noted in the body of the paper, one could employ model fluctuations based on data constraints for fluctuations in mantle potential temperature³² and/or mean plate subduction age³⁰. That goes beyond our scope of demonstrating that self-regulation is robust in the face of thermal-tectonic fluctuations.

Data availability

The data used within this paper can be found in the references provided for the data.

Code availability

The methods detail the steps used within our analysis. They were programmed in a python environment. The corresponding author can be contacted to clarify any questions about the method or algorithms used within the analysis.

Received: 11 March 2022; Accepted: 8 November 2022;

Published online: 26 November 2022

References

- Stevenson, D. J. Styles of mantle convection and their influence on planetary evolution. *Comptes Rendus—Geosci.* **335**, 99–111 (2003).
- Keller, C. & Schoene, B. Statistical geochemistry reveals disruption in secular lithospheric evolution about 2.5Gyr ago. *Nature* **485**, 490–493 (2012).
- Tozer, D. C. The present thermal state of the terrestrial planets. *Phys. Earth Planet. Interiors* **6**, 182–197 (1972).
- Davies, G. F. Thermal histories of convective earth models and constraints on radiogenic heat production in the earth. *J. Geophys. Res.* **85**, 2517–2530 (1980).
- Schubert, G., Stevenson, D. & Cassen, P. Whole planet cooling and the radiogenic heat source contents of the earth and moon. *J. Geophys. Res.* **85**, 2531–2538 (1980).
- Christensen, U. R. Thermal evolution models for the Earth. *J. Geophys. Res.* **90**, 2995–3007 (1985).
- Korenaga, J. Energetics of mantle convection and the fate of fossil heat. *Geophys. Res. Lett.* **30**, 47–63 (2003).
- Jaupart, C., Labrosse, S. & Mareschal, J. C. *Temperatures, Heat and Energy in the Mantle of the Earth* Vol. 7 (Elsevier B.V., 2007). <https://doi.org/10.1016/B978-0-444-53802-4.00126-3>.
- Korenaga, J. Can mantle convection be self-regulated? *Sci. Adv.* **2**, e1601168–e1601168 (2016).
- Seales, J., Lenardic, A. & Moore, W. B. Assessing the intrinsic uncertainty and structural stability of planetary models: 1. Parameterized thermal tectonic history models. *J. Geophys. Res.: Planets* **124**, 2213–2232 (2019).
- Crowley, J. W. & O’Connell, R. J. An analytic model of convection in a system with layered viscosity and plates. *Geophys. J. Int.* **188**, 61–78 (2012).
- Moore, W. B. & Lenardic, A. The efficiency of plate tectonics and nonequilibrium. *Geophys. Res. Lett.* **42**, 9255–9260 (2015).
- Mackwell, S. J., Kohlstedt, D. L. & Paterson, M. S. The role of water in the deformation of olivine single crystals. *J. Geophys. Res.* **90**, 11319 (1985).
- Li, Z. X. A., Lee, C. T. A., Peslier, A. H., Lenardic, A. & Mackwell, S. J. Water contents in mantle xenoliths from the Colorado Plateau and vicinity: implications for the mantle rheology and hydration-induced thinning of continental lithosphere. *J. Geophys. Res.: Solid Earth* **113** (2008).
- Katz, R. F., Spiegelman, M. & Langmuir, C. H. A new parameterization of hydrous mantle melting. *Geochem. Geophys. Geosyst.* **4**, 1–19 (2003).
- Jackson, M. J. & Pollack, H. N. Mantle devolatilization and convection: implications for the thermal history of the Earth. *Geophys. Res. Lett.* **14**, 737–740 (1987).
- McGovern, P. J. & Schubert, G. Thermal evolution of the Earth: effects of volatile exchange between atmosphere and interior. *Earth Planet. Sci. Lett.* **96**, 27–37 (1989).
- Crowley, J. W., G  rault, M. & O’Connell, R. J. On the relative influence of heat and water transport on planetary dynamics. *Earth Planet. Sci. Lett.* **310**, 380–388 (2011).
- Seales, J. & Lenardic, A. Deep water cycling and the multi-stage cooling of the Earth. *Geochim. Geophys. Geosyst.* **21**, 1–22 (2020).
- Seales, J. & Lenardic, A. Uncertainty quantification in planetary thermal history models: implications for hypotheses discrimination and habitability modeling. *Astrophys. J.* **893** (2020).
- Parai, R. & Mukhopadhyay, S. Xenon isotopic constraints on the history of volatile recycling into the mantle. *Nature* **560**, 223–227 (2018).
- Lee, C. T. A. et al. Two-step rise of atmospheric oxygen linked to the growth of continents. *Nat. Geosci.* **9**, 417–424 (2016).
- Eguchi, J., Seales, J. & Dasgupta, R. Great Oxidation and Lomagundi events linked by deep cycling and enhanced degassing of carbon. *Nat. Geosci.* **13**, 71–76 (2020).
- Dong, J., Fischer, R. A., Stixrude, L. P. & Lithgow Bertelloni, C. R. Constraining the volume of earth’s early oceans with a temperature dependent mantle water storage capacity model. *AGU Adv.* **2**, e2020AV000323 (2021).
- Bradley, D. C. Passive margins through earth history. *Earth-Sci. Rev.* **91**, 1–26 (2008).
- Condie, K. C., Pisarevsky, S. A. & Puetz, S. J. LIPs, orogens and supercontinents: the ongoing saga. *Gondwana Res.* **96**, 105–121 (2021).
- Iwamori, H. Transportation of H₂O beneath the Japan arcs and its implications for global water circulation. *Chem. Geol.* **239**, 182–198 (2007).
- Keller, B. & Schoene, B. Plate tectonics and continental basaltic geochemistry throughout Earth history. *Earth Planet. Sci. Lett.* **481**, 290–304 (2018).
- Gerardi, G., Ribe, N. M. & Tackley, P. J. Plate bending, energetics of subduction and modeling of mantle convection: A boundary element approach. *Earth Planet. Sci. Lett.* **515**, 47–57 (2019).
- Karlsen, K. S., Conrad, C. P. & Magni, V. Deep water cycling and sea level change since the breakup of Pangea. *Geochim. Geophys. Geosyst.* **20**, 2919–2935 (2019).
- Chotalia, K., Cagney, N., Lithgow-Bertelloni, C. & Brodholt, J. The coupled effects of mantle mixing and a water-dependent viscosity on the surface ocean. *Earth Planet. Sci. Lett.* **530**, 115881 (2020).
- Van Avendonk, H. J., Davis, J. K., Harding, J. L. & Lawver, L. A. Decrease in oceanic crustal thickness since the breakup of Pangea. *Nat. Geosci.* **10**, 58–61 (2017).
- King, G. & Zeng, L. The dangers of extreme counterfactuals. *Political Anal.* **14**, 131–159 (2006).
- Moore, W. B. & Webb, A. A. G. Heat-pipe Earth. *Nature* **501**, 501–505 (2013).
- Schubert, G., Turcotte, D. L. & Olson, P. *Mantle Convection in the Earth and Planets* (Cambridge University Press, 2001).
- Herzberg, C., Condie, K. & Korenaga, J. Thermal history of the Earth and its petrological expression. *Earth Planet. Sci. Lett.* **292**, 79–88 (2010).

37. Condie, K. C., Aster, R. C. & Van Hunen, J. A great thermal divergence in the mantle beginning 2.5 Ga: Geochemical constraints from greenstone basalts and komatiites. *Geosci. Front.* **7**, 543–553 (2016).
38. Mckenzie, D. & Bickle, M. J. The volume and composition of melt generated by extension of the lithosphere. *J. Petrol.* **29**, 625–679 (1988).
39. Hirschmann, M. M. Mantle solidus: experimental constraints and the effects of peridotite composition. *Geochem. Geophys. Geosyst.* **1**, 2000GC000070 (2000).

Acknowledgements

The authors thank Norm Sleep and Taras Gerya for their reviews of this manuscript and Marc Hirschmann for his review of a previous version of this manuscript. Each reviewer made the ideas and analysis stronger.

Author contributions

J.S., A.L., and M.R. developed the problem and prepared the manuscript. J.S. programmed the model and performed the analysis.

Competing interests

The authors declare no competing interests.

Additional information

Supplementary information The online version contains supplementary material available at <https://doi.org/10.1038/s43247-022-00617-0>.

Correspondence and requests for materials should be addressed to Johnny Seales.

Peer review information *Communications Earth & Environment* thanks Norman Sleep, Taras Gerya for their contribution to the peer review of this work. Primary Handling Editor: Joe Aslin. Peer reviewer reports are available.

Reprints and permission information is available at <http://www.nature.com/reprints>

Publisher's note Springer Nature remains neutral with regard to jurisdictional claims in published maps and institutional affiliations.



Open Access This article is licensed under a Creative Commons Attribution 4.0 International License, which permits use, sharing, adaptation, distribution and reproduction in any medium or format, as long as you give appropriate credit to the original author(s) and the source, provide a link to the Creative Commons license, and indicate if changes were made. The images or other third party material in this article are included in the article's Creative Commons license, unless indicated otherwise in a credit line to the material. If material is not included in the article's Creative Commons license and your intended use is not permitted by statutory regulation or exceeds the permitted use, you will need to obtain permission directly from the copyright holder. To view a copy of this license, visit <http://creativecommons.org/licenses/by/4.0/>.

This is a U.S. Government work and not under copyright protection in the US; foreign copyright protection may apply 2022